Global Scientific JOURNALS

GSJ: Volume 7, Issue 1, January 2019, Online: ISSN 2320-9186
www.globalscientificjournal.com

SYNTHESIS, CHARACTERIZATION & ANTICANCER EVALUATION OF NOVEL CETRIMONIUM TETRAHALO-RUTHENATE/ZNO NANOCOMPOSITE AGAINST MCF-7 BREAST CANCER CELLS

Eman Fayez Said Taha[1], Ola Sayed Mohamed Ali[2], Abdel-Fattah Mohsen Badawi[3], Soheir Saad Korraa[1].

1. Health Radiation Research Department, National Centre for Radiation Research and Technology (NCRRT), Atomic Energy Authority, Cairo, Egypt.
2. Biochemistry Department, Faculty of Pharmacy (Girls), Al-Azhar University, Cairo, Egypt.
3. Applied Chemistry Department, Egyptian Petroleum Research Institute, Cairo, Egypt.

Corresponding author: E-mail: Eman.Fayez@eaea.org.eg

Abstract

Breast cancer is one of the major cases of death in the world. Current treatment of breast cancer is limited to surgery, radiotherapy, and the use of cytotoxic agents, despite their well-known side effects and problems associated with the development of resistance. The discovery and development of novel active chemotherapeutic agents is largely needed. There are some hypotheses to explain the low toxicity and the anticancer properties of ruthenium (Ru) compounds. The present study was conducted mainly to Synthesize, characterize and evaluate the anti-cancer effects of the novel cetrimonium tetrahalo-ruthenate/ZnO nanocomposite (CTR/ZnO NCP) in vitro against human breast cancer cell line (MCF-7). In order to further evaluate Ru complex as potential anti-cancer agent, cetrimonium tetrahalo-ruthenate/ZnO nanocomposite (CTR/ZnO NCP) with general formula [C19H42N+][RuCl3Br-]/ZnO was synthesized by solid-state

grinding, characterized on the basis of TEM, FTIR and XRD and tested for its ability to inhibit breast cancer cells *in vitro*. The complex significantly inhibits *in vitro* the growth of MCF-7 cell line at low concentration, the IC_{50} value in µM range is (0.8). The LD50 value after oral administration is found to be more than 2000 mg kg-1 b.w. which is considered in non-toxic drug category.

Keywords: Ruthenium; Core-shell Nanocomposite; MCF-7 breast cancer cells.

1. Introduction

Breast cancer is the most common cancer amongst women worldwide and is the fifth leading cause of cancer-related mortality overall **(Power *et al.*, 2018).** It also occurs in men with very less frequency compared to women and represents less than 1% of all malignancies in men and only 1% of all breast cancers incident **(Sanguinetti *et al.*, 2016).** Current treatment of breast cancer is limited to surgery, radiotherapy, and the use of cytotoxic agents, despite their well-known side effects and problems associated with the development of resistance **(Mandal&Bishayee, 2015).** Nanotechnology is relatively new and promising scope in the medicine for disease diagnosis, drug delivery at specifc target site, molecular imaging etc. The cancer drug toxicity leads to major complications, several modes for delivery of nanoparticles to tumors, such as liposome mediated drug delivery, biodegradable and biocompatible polymeric nanoparticle delivery **(Kayser *et al.*, 2005)**. The synthesis of nanomaterials remains a scientific challenge, since metal nanoparticles are used in various catalytic applications. There is substantial evidence demonstrating that metal-based reagents are promising candidates for cancer therapies. For example, complexes possessing platinum (Pt), such as cisplatin has been used to treat various cancer types such ovary, stomach, and colon **(Todd&Lippard, 2009)** One of the mechanisms explaining how Pt complexes inhibit cancer cell growth is that they cause interstrand and intrastrand cross-linking of DNA, thereby inhibiting DNA repair or replication **(Baruah *et al.*,**

2004). However, previous studies demonstrated that Pt complexes have severe side effects and generate resistant cancer cells, limiting the effectiveness of this complex. Ruthenium complexes are potent growth inhibitors for various cancer cells such as melanoma, ovarian, and breast **(Betanzos-Lara *et al.*, 2012).**They had been proposed as an alternative to Pt complexes for development of novel anti-cancer drugs. Indeed, several Ru complexes are under phase I or II clinical trials **(Kuhn *et al.*, 2015).** Based on the structure-activity relationship studies, Ru complexes may function to inhibit tumor cells through mechanisms similar to that of cisplatin **(Novakova *et al.*, 2005).** Several antitumor nano drugs are currently being tested in preclinical and clinical trials and show promise in therapeutic and other settings **(Li *et al.*, 2017)**. Core-shell nanoparticles have a core made of a material coated with another material on top of it. In biological applications core-shell nanoparticles have major advantages over simple nanoparticles leading to the improvement of properties such as (i) less cytotoxicity **(Law *et al.*, 2008b),** (ii) increase in dispersibility, bio- and cyto-compatibility, (iii) better conjugation with other bioactive molecules, (iv) increased thermal and chemical stability and so on **(Sounderya&Zhang, 2008).** More elaborately, (i) when the desired nanoparticles are toxic which may cause plenty of trouble to the host tissues and organs. The coating of a benign material on top of the core makes the nanoparticles much less toxic and bio-compatible. Sometimes shell layer not only act as nontoxic layer, but also improve the core material property **(Chatterjee *et al.*, 2014).**

2. Materials and Methods

2.1. Chemicals & Reagents

Zinc Oxide Nanoparticles (ZnO NPs), Ruthenium Trichloride Anhydrous ($RuCl_3$),Cetyltrimethyl Ammonium Bromide (CTAB) and 7,12- Dimethylbenz [a] 1, 2 -benzanthracene (DMBA). All chemicals were kindly purchased from Sigma-Aldrich Company (Sigma Chemical Co, St Louis, MO).

2.2. Synthesis of Novel Cetrimonium Tetrahalo-Ruthenate/Zinc-Oxide Nanocomposite

1. Equimolar amounts of samples were prepared, 2g (0.01M) of anhydrous ruthenium trichloride ($RuCl_3$) and 3.5 g (0.01M) of cetyltrimethyl ammonium bromide (CTAB) were ground in the solid state by hand using an agate mortar and pestle in air for 30 min according to **(Adams *et al.*, 2010),** forming a grayish crystalline powder of cetrimonium tetrahalo - ruthenate complex (CTR).
2. Small droplets of deionized water were added to the complex and mix well for five minutes to aid homogenization and formation of the past.
3. Zinc-oxide nanoparticles (5%; 0.275 g) was added to the past and mix well for 5 minutes.
4. Evaporation of deionized water occurred and samples were dried in vacuum or in the oven at 40 ^{O}C forming the corresponding cetrimonium tetrahalo-ruthenate/ZnO nanocomposite (CTR/ZnO NCP). This method was recommended by **Prof. Dr. Abdelfattah Badawi**, Petroleum Research Institute, Cairo, Eggypt.
5. The molecular weight of each material and prepared samples were showed in Table (1).

Table 1. Molecular weight of each material and prepared samples

Sample	Molecular weight (g M^{-1})
ZnO NPs	81.38
CTAB	364.45
$RuCl_3$	207.43
CTR	571.88*
CTR/ZnO NPs	653.26*

*Molecular weight (gram per mole) of prepared compounds was calculated from addition reaction of control samples.

2.3. Characterization

i. Transmission Electron Microscopy (TEM)

Transmission electron microscopy (TEM) images were obtained from a JEOL JEM-2100 instrument operated at an accelerating voltage at 200 kV at Petroleum Research Institute, Cairo. Samples were prepared by dropping the particles while still in solution onto carbon-coated copper grids and air-drying before measurement. An extremely small amount of material is suspended in a solvent (Ethanol). Brief (15-20 m) ultrasonication was used to disperse particles, and then the suspension (10 µl) was transferred to TEM carbon-coated grids using a micromanipulator and allowed to air dry before viewing **(Vierrether *et al.*, 2016).** The particle size was analyzed using ImageJ software, National Institutes of Health **(Chung *et al.*, 2014).**

ii. The X-Ray Diffraction (XRD)

The X-ray diffraction (XRD) patterns of the synthesized nanoparticles were recorded using a PANalytical X'pert PRO x-ray diffractometer with Cu Kα (λ=1.5406 Å) radiation over a scanning interval (2θ) from 4° to 80° at Petroleum Research Institute, Cairo. The average crystallite sizes were estimated using the Scherrer formula from the X-ray line broadening **(Xiong *et al.*, 2006).**

- **Particle Size Measurements**

Crystal structures are solved by analyzing the intensities of diffracted X-ray beams. The three highest peaks was used to estimate the mean crystallite size D from Scherrer equation **(Jayasuriya *et al.*, 2013)**, as given D = Kλ/ (β cos θ) **(Nair *et al.*, 2014)**, in which; K is consonant (0.9), λ is wavelength (Cu Kα) (λ=1.5418 Ao), β is full width at the half-maximum (FWHM) and θ is diffraction angle by radian.

iii. Fourier-transform infrared spectroscopy (FTIR)

The presence of functional groups is analyzed by Fourier-transform infrared spectroscopy (FTIR), model: Nexus 670 (Nicollet-Madison-WIUSA) in the mid-infrared region 4000-400 cm-1 at National Research Centre. The samples were mixed uniformly with potassium bromide at 1:100 (sample: KBr) ratio, respectively into an agate mortar. They were ground to fine powder. The die was put together with the powder into the Qwik Handi Press. The powder was pressed for 2 min to form a pellet. The collar together with the pellet was put onto the sample holder **(AbdElhady, 2012).**

2.4. *In Vitro* Cytotoxicity Study (MTT Test)

The *in vitro* anticancer cytotoxic activities of free ZnO NPs, CTAB, $RuCl_3$, Cetrimonium tetrahaloruthenate (CTR) and its combination with ZnO NPs

(CTR/ZnO NPs), were investigated against human breast cancer cell line (MCF-7) obtained from Faculty of Pharmacy for Boys-Al Azhar University, Cairo, Egypt, using 3-(4,5-dimethylthiazol-2-yl)-2,5-diphenyltetrazolium bromide cell viability assay (MTT assay) for various concentrations **(Rahimi *et al.*, 2015).** The cells were grown in RPMI-1640 medium supplemented with FBS. Stock solutions of each material was prepared and diluted with different concentrations (1000, 100, 10, 1, 0.1,0 μM) using the cell culture medium. Cells (1×10^5/well) in 0.2 mL of medium were plated in 96-well plates. Then it was kept under 5% CO_2 incubator for 24 h. The various concentrations of the samples in 0.1% DMSO were added for 24 h at 5% CO2. The sample solution was removed and 20 μl /well (5 mg mL^{-1}) of 0.5% MTT in phosphate-buffered saline solution was added. Then 1 mL of DMSO was added after 4 h of incubation. At 540 nm viable cells were determined. The concentration required for a 50% inhibition of viability (IC_{50}) was determined graphically (Nonlinear regression graph was plotted between % cell viability and concentration, the IC_{50} was determined using graph pad prism 5 software) Significant was expressed by Bonferroni test, two ways ANOVA. The samples effect was determined on the proliferation of MCF-7 cell was expressed as the % cell viability, using below formula:

$$\%\text{Cell viability} = A_{540} \text{ of treated cells} / A_{540} \text{ of control cells} \times 100\%$$

2.5. Acute Toxicity Study (Determination of LD_{50})

Determination of LD_{50} (the dose which has proved to be lethal to 50% of the tested group of animals) is usually an initial step in the assessment and evaluation of the toxic characteristics of a substance **(Akhila *et al.*, 2007).** Seven groups containing five Female albino rats in each, weighing (100-120 g) obtained from the breeding unit of The National Center for Radiation Research and Technology (NCRRT), Cairo, Egypt, were used through these experiments. Rats were fasted for 18 h prior to dosing. The compound was administered once orally using oral feeding needle

to the rats. The volume of the dose depends on the size of the animals. In rodents, it should not exceed 1 mL/100 g b.w. **(Ghosh, 1984).**

- **Estimation of the Dose Range and Percentage of Mortalities**

An approximate LD_{50} can be determined by the "staircase method" using two animals and increasing the doses of CTR/ZnO NPs. Seven doses were given orally once and different doses (control, 200, 300, 400, 500, 1000, 2000 mg kg^{-1}) to 7 groups of rats (5 rats in each group) for the determination of LD_{50} of the complex starting from 0% mortality to 100% mortality **(Randhawa, 2009).** The animals were observed for 2 h and then at 4^{th}, 6^{th}, and 24^{th} h for any toxic signs or symptoms, change in behavior or physical activities. After 24^{th} h, the numbers of deceased rats in each group were counted and the percentage of mortality was calculated. The LD_{50} of the studied compound were determined as described by **(Kärber, 1931).**

- **Calculation of Median Lethal Dose (LD_{50})**

For each rat, the observation was made for 24 h; symptoms of toxicity and rate of mortality in each group were noted. The arithmetic method of Karber **(Kärber, 1931),** was used for the determination of LD_{50}.

$$\mathbf{LD50 = LD100 - \sum (a \times b) / n}$$

Where;

- n = Total number of animal in a group.
- a = The difference between two successive doses of administered extract / substance.
- b = The average number of dead animals in two successive doses.
- LD_{100} = Lethal dose causing the 100% death of all test animals.

Hodge and Sterner scale (Table 2) was used for the evaluation of toxicity with the help of LD_{50} **(Hodge&Sterner, 2005).**

Table 2. Hodge and sterner toxicity scale

No.	Term	LD_{50} (Rat, Oral)
1	Extremely Toxic	Less than 1 mg kg^{-1}
2	Highly Toxic	1 - 50 mg kg^{-1}
3	Moderately Toxic	50 - 500 mg kg^{-1}
4	Slightly Toxic	500 - 5000 mg kg^{-1}
5	Practically Non Toxic	5000 - 15,000 mg kg^{-1}

Statistical Analyses

Nonlinear regression graph was plotted between % cell viability and concentration, the IC_{50} was determined. Analysis of variance (ANOVA; followed by Bonferroni or Tukey, Post Hock test), was used according to the specific context, as stated in figure legends. A p-value of less than .05 was considered statistically significant. All tests were performed in GraphPad Prism 5.01 software for Windows (GraphPad Software, San Diego California USA, www.graphpad.com). Results for FTIR and XRD were performed using SigmaPlot 12.5 software for Windows.

3. Results

3.1. Synthesis of CTR/ZnO NCP by solid state reaction

Cetyltrimethylammonium bromide was positively charged with a tetrahedral head and a hydrophobic tail, a new cetrimonium tetrahalo-ruthenate with general formula $[C_{19}H_{42}N^{+}][RuCl_3Br^{-}]$ was obtained. It contains a pair of ions, one organic

(CTA^+) cation, and one inorganic ($RuCl_3^-$) anion, ion pairs were formed initially by electrostatic interaction.

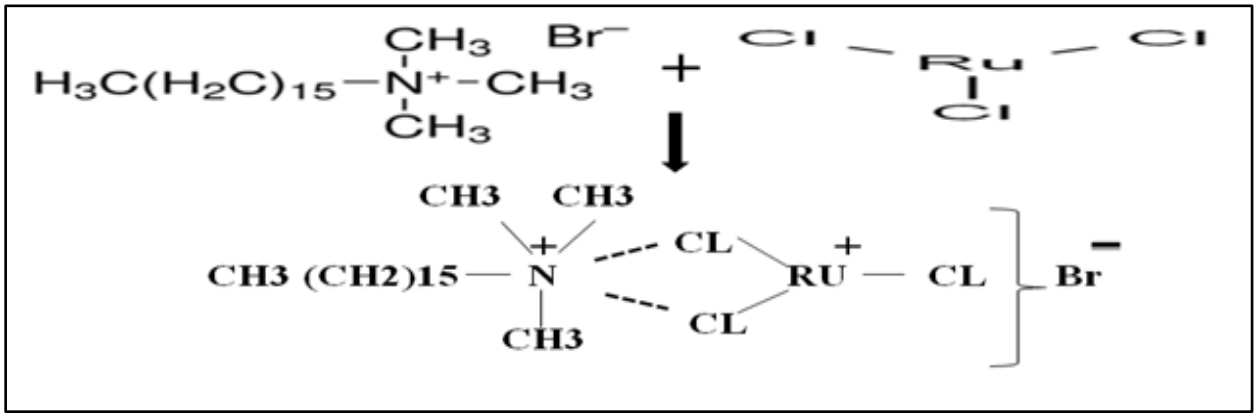

Scheme 1. Illustration of the structure of CTR complex

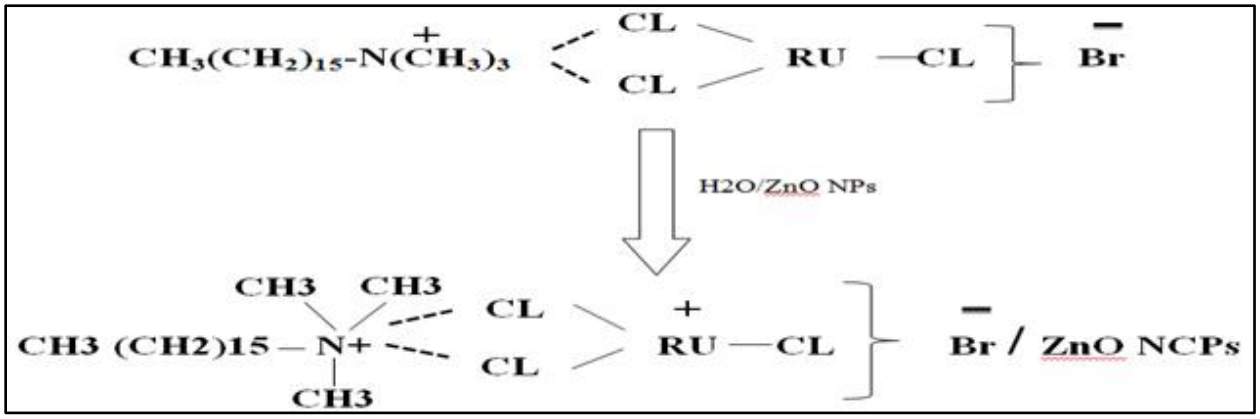

Scheme 2. Illustration of the structure of the CTR/ZnO NCP.

3.2. Characterization of CTR/ZnO NCP

I. Transmission Electron Microscopy

Representative TEM images of the CTR/ZnO NCP were shown in Fig. (2). The TEM images showed the morphology of the core-shell nanostructures (a-d). A clear difference in contrast, can be observed between the CTR core and the ZnO shell due to the difference in atomic number and thus attenuation of electrons. It is clear that essentially every cube or spherical shell contained one CTR nanocrystal

seed in its center. The ZnO shell was evenly deposited on the CTR seeds, forming a complete coating on the CTR core. The darker CTR core (in the center) surrounded by a lighter ZnO shell can also be easily distinguished from the TEM images. Images indicated that the CTR/ZnO NCP were spherical or nanocube with a CTR-core diameter of about 35-85 nm and ZnO shell thickness of about 8-10 nm. The results indicated that the average particle size was 15.15 nm. There was a good correspondence between CTR/ZnO NCP size shown in the TEM and that calculated from XRD spectrum by Scherrer formula.

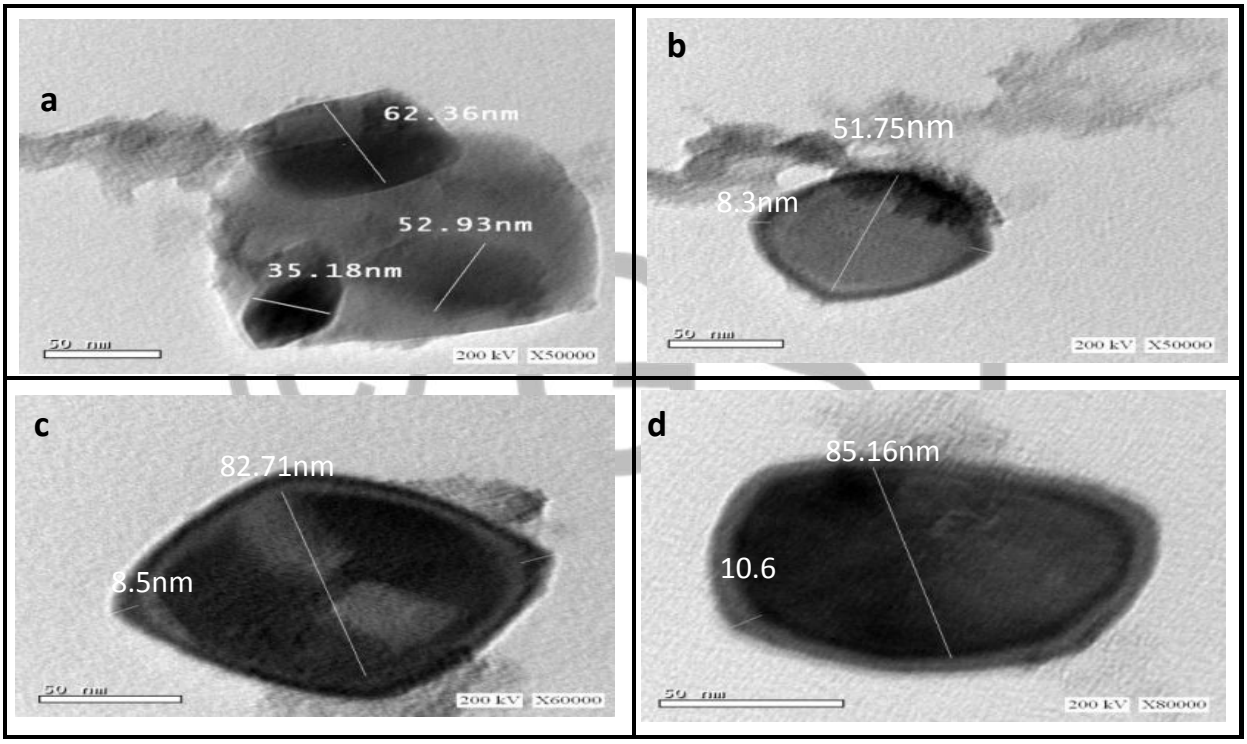

Figure 2. TEM images of CTR/ZnO core-shell nanoparticles; Scale bars were 50 nm.

II. The X-Ray Diffraction Pattern

The peaks at 6.87, 20.52 and 21.42° were the characteristic peaks of CTAB with a monoclinic lattice structure (JCPDS# 30-1746), which indicated that the sample is phase-pure as no peaks from other CTAB phases or impurities were observed. The results in Fig. (3) showed that the XRD patterns of the CTR appeared at 20.55,

24.02 and 6.85 were very similar to that of CTAB without clear diffraction peaks of $RuCl_3$. The CTR diffraction peaks in the XRD spectrum were a little broader than CTAB and their positions were shifted to the right. The basal spacing of CTAB was 12.92 Å, while the spacing of CTR was decreased to 4.31 Å. In addition, the diffraction peaks of CTR/ZnO NCP appeared at 21.22, 34.70 and 27.51°, where the planes became broader compared to that of CTR. The basal spacing of CTR/ZnO NCP was 4.18 Å and were no diffraction peaks for ZnO NPs in the XRD pattern in the wide-angle range.. It was clear that the intensity of the peaks belonging to the CTR in the diffraction pattern of CTR/ZnO NCP was lower than pure CTR.

- **Particle Size Measurements**

The results in Table (3) showed the particle size of each material to the highest peak. It was noticed that by the addition of CTAB to $RuCl_3$, the obtained CTR average crystal size got smaller. Furthermore, after the addition of ZnO NPs to the CTR complex, the obtained average crystal size of CTR/ZnO NCP was decreased from 52.9 nm to 11.97 nm.

Table 3. The average crystallite size of each material based Scherrer formula.

Samples	2θ (deg)	FWHM (deg)	D (nm)
ZnO NPs	34.07	0.19	41.86
CTAB	16.26	0.16	51.20
$RuCl_3$	22.52	0.08	110.3
CTR	17.14	0.15	52.9
CTR/ZnO NCP	27.82	0.71	11.97

nm =A°/10; Radian= degree * π /180 .D= average crystal size (nm).

*Table represented the average data of three strongest peaks.

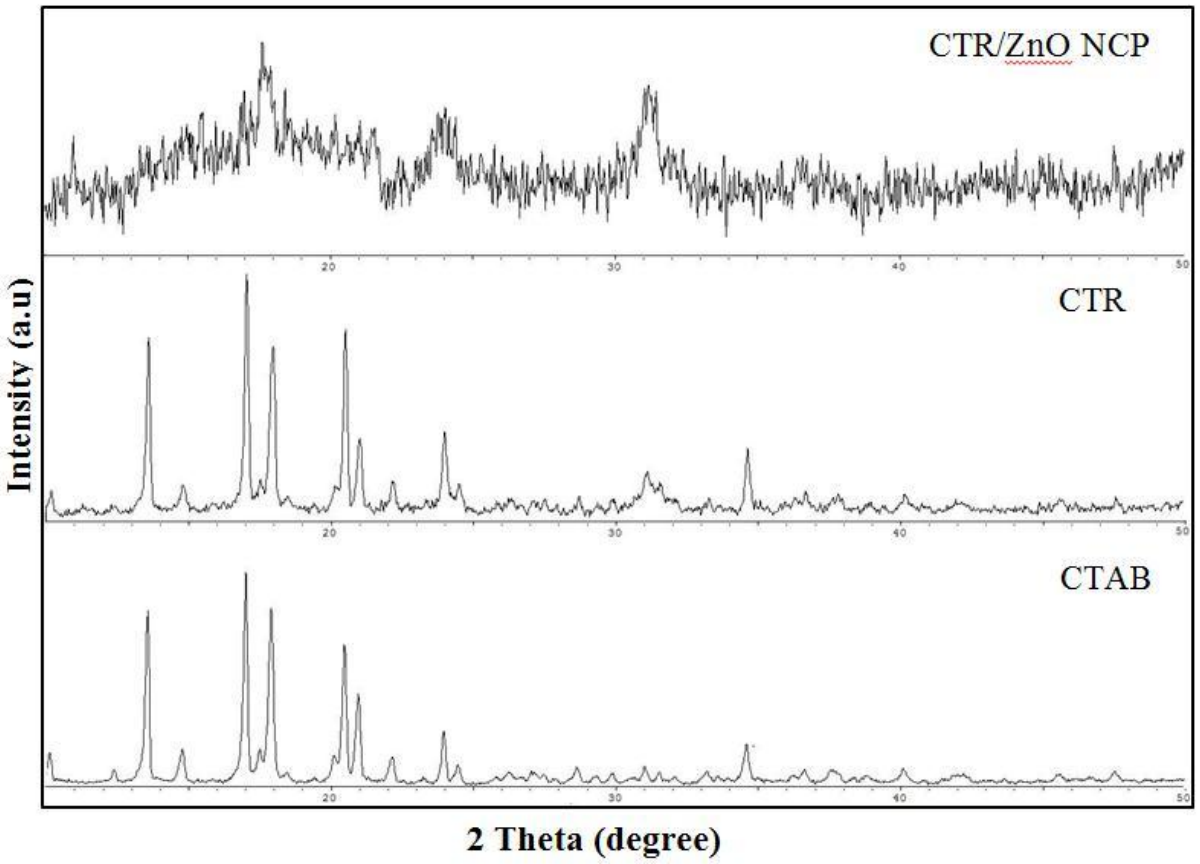

Figure 3. The X-ray diffraction patterns of CTAB, CTR & CTR/ZnO NCP.

III. Fourier Transform Infrared Spectroscopy (FTIR)

The FTIR spectrum of the CTAB, CTR and CTR/ZnO NCP samples acquired in the range of 4000-400 cm^{-1} was shown in Table (4) & Fig. (4). The binding of the metal with the ammonium ions of the CTAB established through their M-N stretching irrespective of the metal. There were several stretching bands observed in the spectra which were 3424, 3015, 2918, 2849, 962, 910 and 724 cm^{-1} that represent different characteristic groups of CTAB. The bands at 3424, 3015 and 1625 cm^{-1} respectively assigned for the quaternary compound of the ammonium salt. Similarly, the presence of alkyl chain was confirmed through the characteristic peak noticed at 2918 and 2849 cm^{-1} correspond to the stretching modes of

methylene groups' νas (CH_2) and νs (CH_2), respectively which confirmed the presence of CTAB. The band observed at 1474 cm^{-1} is assigned also to N^+-CH_3 head group methylene scissoring vibration. The band at 3424 cm^{-1} corresponds to (N-H) stretching mode of vibration was shifted to 3426 cm^{-1} in the FTIR spectra of CTR and 3444 cm^{-1} for CTR/ZnO NCP, while the peak noticed at 3015 cm^{-1} correspond to -C-N^+)$CH_3)_3$ in CTAB was shifted to 3019 cm^{-1} in the FTIR spectra of CTR and 3029 cm^{-1} for CTR/ZnO NCP. After attachment of $RuCl_3$ to CTAB, the peak at the C-N stretching was shifted from 1042 cm^{-1}) CTAB) to 1033 cm^{-1} (CTR) and the emergence of peak of Ru complex at 1135 cm^{-1}. The strong peak at 724 which assigned to CH_2 rocking, 906 and 958 cm^{-1} which assigned to C-N stretching for pure CTAB was either broadened or shifted in the case of CTR. Moreover, the band at 455 cm^{-1} could be assigned to metal halide stretching mode (Ru-N) from the chelating of CTAB with metallic ions, while the band located at 546 cm^{-1} was correlated to the stretching mode of Zn-O.

Table 4. Stretching wavenumber values of the CTAB, CTAB stabilized metal & CTR/ZnO NCP obtained using the FTIR spectroscopy.

Peak	CTAB	CTR	CTR/ZnO NCP
(N-H) stretching	3424	3426	3444
(N-H) bending	1625	1620	1623
N^+ CH_3 C-H stretching	3015	3019	3029
CH_2 stretching (*vas*)	2918	2917	2918
CH_2 stretching (*vs*)	2849	2849	2851
N^+ CH_3 head group methylene scissoring	1474	1465	1463
N^+ CH_3 head group methylene rocking	724	716	705
N^+ CH_3 head group methylene wagging	1401		
C-N^+ stretching	1042	1033	
C-N^+ stretching	962	964	962
C-N^+ stretching	910	910	907
Ru-N stretching vibration		455	
ZnO stretching			546

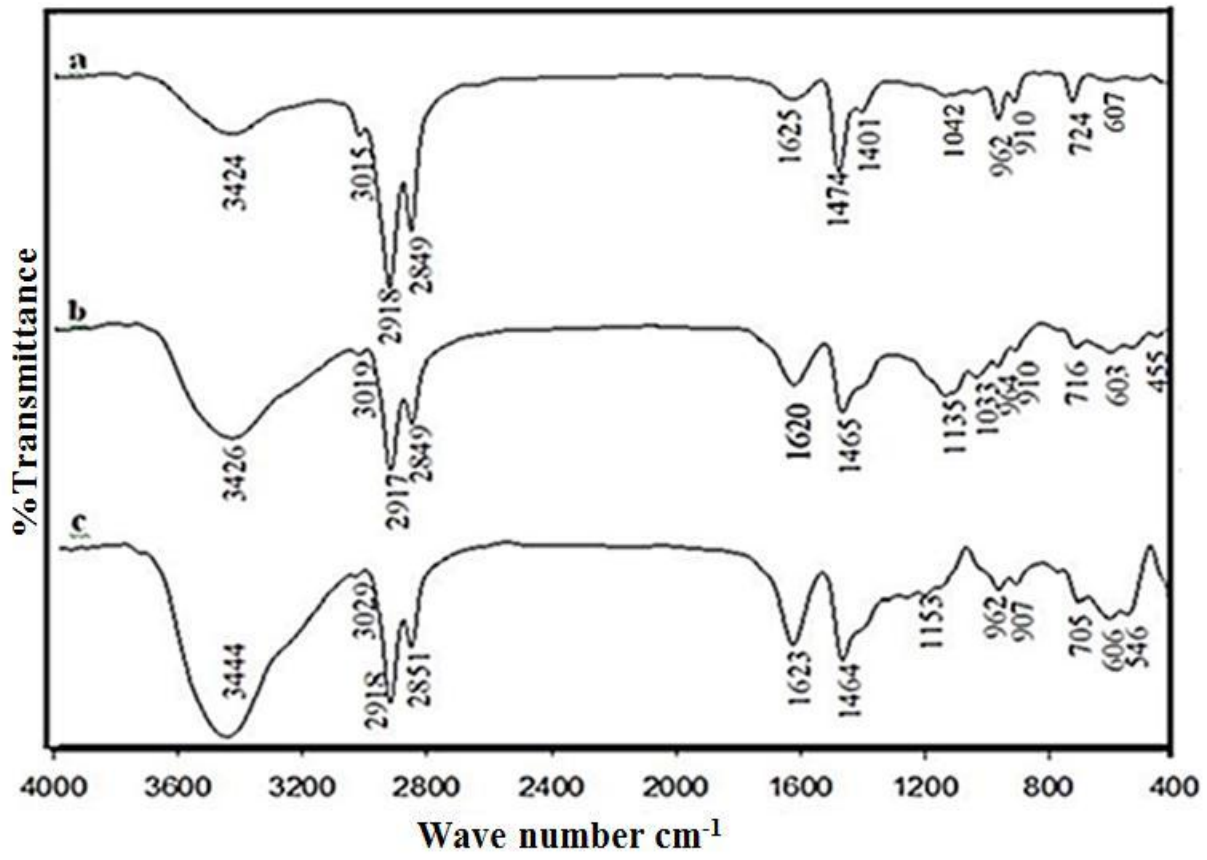

Figure 4. The FTIR spectrum of a) CTAB; b) CTR & c) CTR/ZnO NCP.

3.2. *In vitro* Study

The in vitro anticancer cytotoxic activities of test materials were investigated on human breast cancer cell line (MCF-7) using MTT assay for various concentrations. The results in Table (5) showed that the exposure of MCF-7 cells to all test materials at the various concentrations for 24 h significantly reduced the cell viability in a concentration dependent manner. As the concentration increased the cell viability (%) significantly decreased. For CTR/ZnO NCP there was a significant decrease ($P < 0.01$) in cell viability from 100 to 76.34 % at 0.1 µM as compared to CTAB. However, the cell viability at the highest concentrations (1, 10, 100 and 1000 µM) was not significant ($P > 0.05$).

Moreover, data indicated that there was a high significant decrease ($P<0.001$) in cell viability (%) of CTR/ZnO NCP from 0.1 to 1000 µM when compared to ZnO NPs and RuCl3, while non-significant decrease ($P>0.05$) in cell viability (%) was shown at 100 and 1000 µM as compared to CTR. Data generated were used to plot a dose response curve of which the concentration of test compounds required to kill 50% of cell population (IC_{50}) was determined. The cytotoxic activity was expressed as reduction of cell viability relative to control. Cytotoxic activity was expressed as the mean IC50 of three independent experiments. Interestingly, the results were represented in Table (6) and Fig. (4) showed growth inhibition of MCF-7 cells in a dose dependent manner when treated with the novel CTR/ZnO NCP which exhibited the strongest in vitro anticancer activity against MCF-7, where it recorded the lowest IC50 value (0.80 µM) comparable to that of ZnO NPs (395.2 µM), CTAB (1.04 µM), RuCl3 (>1000 µM) and CTR (0.89 µM) against MCF-7 breast cancer cell line.

Table 5. *In vitro* cytotoxic activity at different concentrations of test materials against MCF-7 cell line using the MTT assay test.

Conc (µM)	Cell viability (%)*				
	ZnO-NPs	**CTAB**	**$RuCl_3$**	**CTR**	**CTR/ZnO NCP**
0	100 ±1.96	100 ±1.96	100 ±1.96	100 ±1.96	100 ±1.96
0.1	96.14±2.10	95.99±0.55	79.21±0.50	83.82±2.79	76.34±2.85
1	86.16±0.81	54.49±2.37	76.1±2.31	42.78±1.52	37.79±1.18
10	85.33±0.15	12.69±1.90	72.48±1.11	8.31±0.27	5.89±0.13
100	77.92±2.01	2.04±0.13	72.10±0.68	2.19±0.07	1.96±0.07
1000	13.75±0.52	1.89±0.19	55.55±3.46	1.88±0.07	1.81±0.13

* Data expressed as the mean value of cell viability ± SEM
Results were expressed by Bonferroni test, two ways ANOVA.

Table 6. The IC_{50} values (µM) obtained by test compounds at different concentrations against MCF-7 cells using MTT assay.

Test compounds	**ZnO NPs**	**CTAB**	**$RuCl_3$**	**CTR**	**CTR/ZnO NCP**
IC_{50} (µM)*	395.2	1.04	> 1000	0.89	0.80
R^2	0.78	0.98	0.51	0.98	0.97

*The Nonlinear regression graph was plotted between % cell viability and concentration, the IC50 was determined.

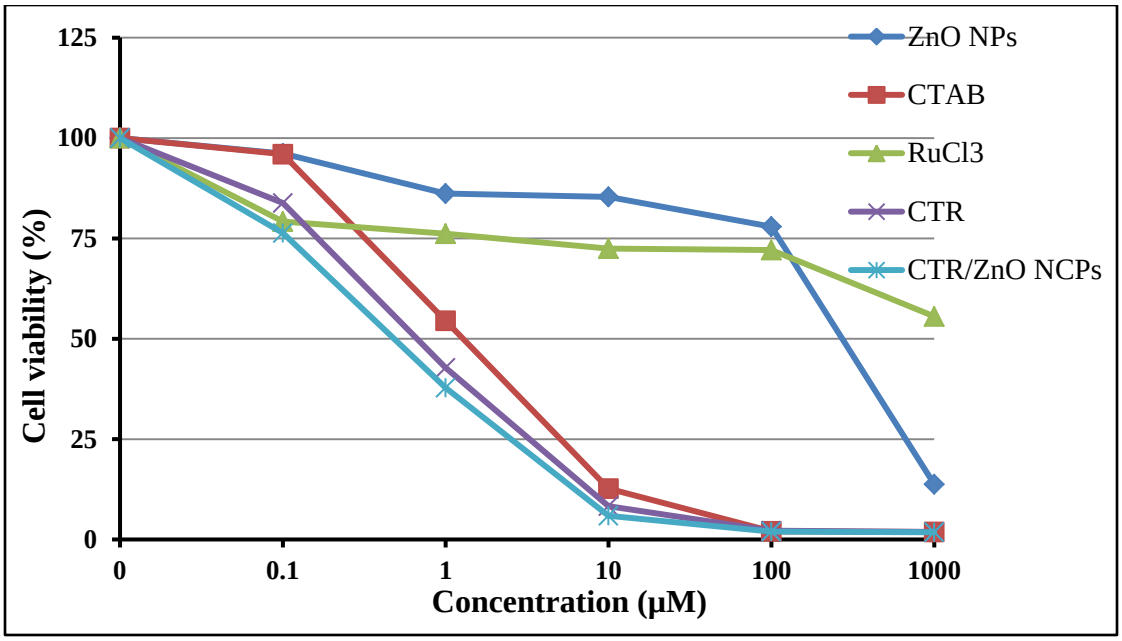

Figure (5): *In vitro* cell viability assay at different concentrations of test materials against MCF-7 breast cancer cell line.

*Statistical analysis was performed by two ways ANOVA, Bonferroni test.

3.3. *In vivo* studies

3.3.1. Determination of Median Lethal Dose Value of CTR/ZnO NCP

The incidence of mortality in rats by CTR/ZnO NCP was presented in Table (7). From the experiment, the results revealed that the CTR/ZnO NCP had not been found to be toxic even at 200 mg/kg or 2000 mg/kg as shown. The animals received 2000 mg/kg orally was not found to cause any mortality. The LD50 value of CTR/ZnO NCP after oral administration was found to be more than 2000 mg/kg b.w. As a result, 2000 mg/kg b.w. of complex was considered approximately half its lethal dose that is the dose that did not cause any signs of toxicity or abnormal symptoms. The CTR/ZnO NCP at sublethal dose equivalent to 1/20th of LD50 were suspended in distilled water and administered to animals by gavage in a volume of 1 ml /rat.

Table 7. Toxicological study of different doses of CTR/ZnO NCP administered orally in rats.

Groups	Dose/Day	Mortality (X/N)	Symptoms (2h)
Group I	D. H2O (200 ml Kg^{-1})	0/5	Nil
Group II	200 mg kg^{-1}	0/5	Nil
Group III	300 mg kg^{-1}	0/5	Nil
Group IV	400 mg kg^{-1}	0/5	Nil
Group V	500 mg kg^{-1}	0/5	Nil
Group VI	1000 mg kg^{-1}	0/5	Nil
Group VIII	2000 mg kg^{-1}	0/5	Nil

*X: number of dead animals, N: total number per group.

4. Discussion

Breast cancer is the most common cancer among women and the second leading cause of cancer-associated deaths in humans worldwide **(Ferlay *et al.*, 2015).** The synthesis of nanomaterials remains a scientific challenge, since metal nanoparticles are used in various catalytic applications. There was substantial evidence demonstrating that metal-based reagents were promising candidates for cancer therapies **(Todd&Lippard, 2009).** Up to now more than 1000 analogues of cisplatin (CP) have been synthesized and tested preclinically to develop compounds with higher anti-neoplastic activity and lower side-effects. Only a few platinum complexes showed definite advantages over CP in clinical trials **(Warrell, 1995).** In the present study, cetrimonium tetrahalo-ruthenate/Zinc-oxide nanocomposite (CTR/ZnO NCP) with general formula; $[C_{19}H_{42}N^{+}]$ $[RuCl_3]$ Br^{-} /ZnO NCP as a new derivative, with speculated reduced risk of toxicity was synthesized by solid state reaction. These solid-state methods are more efficient than the traditional ones, or give better selectivity, or both **(Adams *et al.*, 2010).**

The prepared nanoparticles were confirmed by various characterization studies such as transmission electron microscopy (TEM), Fourier-transform infrared spectroscopy (FTIR) and X-ray powder diffraction (XRD). Images of TEM indicated that the CTR/ZnO core shell nanoparticles, were spherical or nanocube with a cetrimonium tetrahalo-ruthenate (CTR)-core diameter of about 35-85 nm and ZnO shell thickness of about 8-10 nm and the results indicated that the average particle size was 15.15 nm. There was a good correspondence between CTR/ZnO nanoparticles size shown in the TEM and that calculated from XRD spectrum by Scherrer formula. In biological applications core-shell nanoparticles have major advantages over simple nanoparticles leading to the improvement of properties such as (i) less cytotoxicity **(Law *et al.*, 2008a)**, (ii) increase in dispersibility, bio - and cyto -compatibility, (iii) better conjugation with other bioactive molecules, **(Sounderya&Zhang, 2008).** Sometimes shell layer not only act as nontoxic layer, but also improve the core material property **(`Chatterjee *et al.*, 2014).** Furthermore, the FTIR spectrum of the CTAB, CTR and CTR/ZnO NCP samples acquired in the range of 4000-400 cm^{-1} was shown in (Fig. 3). The binding of the metal with the ammonium ions of the CTAB established through their M-N stretching irrespective of the metal. The CTAB surfactant is adsorbed with the head-group pointing to the surface and the hydrocarbon chain is adsorbed flat with the tail running parallel to the surface **(Koglin *et al.*, 1997).** There were several stretching bands observed in the spectra which were 3424, 3015, 2918, 2849, 962, 910 and 724 cm^{-1} that represent different functional groups of CTAB. The band at 3424, 3015 and 1625 cm^{-1} respectively assigned for quaternary compound of ammonium salt, which were formed by the reaction of CTAB with $RuCl_3$, these results were in agreement with **(Murugan *et al.*, 2015).** The band at 2918, 2849 and 1474 cm^{-1} respectively assigned for CH_2 and CH_3 stretch of alkane, besides CH bending occurs at 1474 cm^{-1} which were formed by solid state grinding. The band

455 cm^{-1} could be assigned to metal halide stretching mode from the chelating of CTAB with metallic ions, besides strong adsorption bands appear at 962 cm^{-1} and can be assigned to metal ions in the dried powder. These results were in agreement with **(Ahmed *et al.*, 2017).** Moreover, these results were contradictory to previous studies that showed that the band of medium intensity near 490 cm^{-1} assigned by other workers to the Ru-N stretching vibration **(Quinby&Feltham, 1972).** The band at 3424 cm^{-1} corresponds to (N-H) stretching mode of vibration was shifted to 3426 cm^{-1} in the FTIR spectra of CTR and 3444 cm^{-1} for CTR/ZnO NCP. The absorption peaks at 2918 and 2849 cm^{-1} correspond to the stretching modes of methylene groups' νas (CH_2) and νs (CH_2), respectively which confirm the presence of CTAB. The peak noticed at 3015 cm^{-1} correspond to -C-N^+)CH3)3 in CTAB was shifted to 3019 cm^{-1} in the FTIR spectra of CTR and 3029 cm^{-1} for CTR/ZnO NCP, this observation confirmed the stabilization of the metal with CTAB. Similar results were observed by Murugan et al. **(Murugan *et al.*, 2015).** Similarly the presence of alkyl chain irrespective of catalyst was confirmed through the characteristic peak noticed at 1474 cm^{-1} for CH_2 and CH_3 stretching. The band observed at 1474 cm^{-1} is assigned to N^+-CH_3 head group methylene scissoring vibration. The bond in these complexes is a type of ionic interaction. This type of interaction caused the shift of both (CH_3) and (CH_2) groups. Similar results were observed by **(Ezzoukhry *et al.*, 2012).** Further, the band at 1042 cm^{-1} is assigned to the C-N group, After attachment of $RuCl_3$ to CTAB, the peak at the C-N stretching was shifted from 1042 cm^{-1}) CTAB) to 1033 cm^{-1} (CTR) and the emergence of some peaks of Ru complex at 1135 and 1033 cm^{-1} was in well conformity to the successful attachment of complex to CTAB confirms that the metal had been attached to the Nitrogen by vanderwalls attraction. The strong peaks at 724, 906 and 958 cm^{-1} for pure CTAB were either broadened or shifted in the case of CTR which indicated an interaction of CTAB with $RuCl_3$. Results in

the present study were in agreement with **(Murugan *et al.*, 2015).** It had been previously reported that the band located at 460-560 cm^{-1} was correlated to the stretching mode of Zn-O while the peak which was observed from 400 to 500 cm^{-1} was due to Zn–O vibrations of ZnO NPs **(Sadollahkhani *et al.*, 2014).** The results of the IR spectrum of ZnO nanostructures are generally influenced by particle size and morphology **(Ismail, 1991).** Moreover, the absorption peaks at 659 cm^{-1} and 465 cm^{-1} which were due to the attachment of amide group and stretching mode of ZnO **(Bhadra *et al.*, 2011).** In addition to these results, the characteristic peaks of CTR/ZnO NCP were shifted to lower wavenumber, the wide peak at 3426 cm^{-1}, corresponding to the stretching vibration of amino and amide groups, moved noticeably to higher wavenumbers 3444 cm^{-1}, and became broader and stronger, which indicated the strong interaction between these groups, this was in agreement with **(AbdElhady, 2012).** Present data demonstrated that in the IR spectra there was a general shift to lower wavenumbers and broadening of the NH_2 vibrations. The shifting and broadening were indicative of an increase in hydrogen bonding in the complexes. This was in contrast to coordination metal – CTAB complex, where a decrease in hydrogen bonding was observed (shift to higher wavenumbers). In this complexe a marked increase of intensity of the NH_2 bands was also observed and attributed to hydrogen bond weakening due to covalent metal – CTAB bonding that existed, these results were in agreement with **(Brennan, 2005).** The XRD analysis elucidated that the peaks at 6.87, 20.52 and 21.42 ° were the characteristic peaks of CTAB with a monoclinic lattice structure (JCPDS# 30-1746). Results showed that the XRD patterns of CTR were very similar to that of CTAB without clear diffraction peaks of $RuCl_3$. The CTR diffraction peaks in the XRD spectrum were broadened, and their positions were shifted to the right. This indicated a possible strong interaction between CTAB and $RuCl_3$. So it can be concluded that the addition of $RuCl_3$ reduced crystallinity of

CTAB, this is in accordance with **(Rilda *et al.,* 2015).** However, there was no diffraction peak for ZnO nanoparticles in the XRD pattern in the wide-angle range, which implied that the ZnO particles were either very small or amorphous, these results were in agreement with **(Zhou *et al.,* 2013).** On the other hand, the intensity of the peaks belonging to the CTR in the diffraction pattern of CTR/ZnO NCP were lower than pure CTR. This may be attributed to the fact that decreasing the peak intensities can be a sign of increasing the covering of the CTR with another material. Similar results were observed by **(Rilda *et al.,* 2015).** Interestingly, the present results (Table 4 & Fig. 4) showed growth inhibition of MCF-7 cells in a dose dependent manner when treated with the novel CTR/ZnO NCP which exhibited the strongest *in vitro* anticancer activity against MCF-7, where it recorded the lowest IC_{50} value (0.80 µM) comparable to that of ZnO-NPs, CTAB, $RuCl_3$ and CTR against MCF-7 breast cancer cell line. These results were in agreement with **(Ypsilantis *et al.,* 2014),** who stated that ruthenium complex showed high cytotoxicity against MCF-7 cancer cell line, with IC_{50} values ranging 0.464–0.925 µM, which can be attributed to a non-classical mechanism for metal based anticancer agents. The 3-(4,5-dimethylthiazol-2-yl)-2,5-diphenyltetrazolium bromide) MTT (pale yellow) cytotoxicity assay is based on the ability of mitochondrial dehydrogenase enzymes from viable cells to cleave the tetrazolium rings of MTT. Dark purple formazan crystals were formed, which are largely impermeable to cell membranes and accumulate within healthy cells. The level of formazan produced is directly proportional to the number of surviving cells. Screening potential drugs for in-vitro toxicity is very important in the drug discovery process. Toxicity of cells can lead to either necrosis or apoptosis along with other changes in nuclear morphology, mitochondrial function and cell permeability **(Al-Jailawi *et al.,* 2015).** It had been previously reported that one of the mechanisms explaining how Pt complexes inhibit cancer cell growth is that

they cause interstrand and intrastrand cross-linking of DNA, thereby inhibiting DNA repair or replication **(Baruah *et al.*, 2004).** However, previous study demonstrated that Pt complexes have severe side effects and generate resistant cancer cells, limiting the effectiveness of this complex. On the other hand, the ruthenium complexes are potent growth inhibitors for various cancer cells such as melanoma, ovarian, and breast **(Betanzos-Lara *et al.*, 2012).** Ruthenium complexes have been proposed as an alternative to Pt complexes for development of novel anti-cancer drugs. Indeed, several Ru complexes are under phase I or II clinical trials **(Kuhn *et al.*, 2015).** Based on the structure-activity relationship studies, Ru complexes may function to inhibit tumor cells through mechanisms similar to that of CP **(Novakova *et al.*, 2005).** In acute toxicity studies, It had become evident that animal mortality could be explained via simple observation of clinical signs followed by necropsy **(Dandekar *et al.*, 2010).** The results of the LD_{50} values of the CTR/ZnO NCP were summarized in (Table 3-5). The mortality of the animals was calculated against several oral administration of CTR/ZnO NCP at an interval of 24 h and the dose produced 50% mortality in animals were calculated with the help of standard formula as described by Kärber, **(Kärber, 1931).** Present data represented that the LD_{50} value of the novel CTR/ZnO NCP was found to be more than 2000 mg/kg body weight. According to Hodge and Sterner, toxicity scale, CTR/ZnO NCP is said to be in non-toxic drug category **(Hodge&Sterner, 2005)**. More than three decades ago, similar results were observed which described substances are to be safe and or of low toxicity if they have LD_{50} of 1,000 mg/kg body weight after an oral route administration **(Kura *et al.*, 2015).** However, no animals exhibited any sign of clinical toxicity; the treatment did not alter their feeding or water intake so it was concluded that CTR/ZnO NCP was safe or practically non-toxic when administered orally.

5. Refferances

1. `Chatterjee K., Sarkar S., Jagajjanani R.K. & Paria S.(2014): Core/shell nanoparticles in biomedical applications. Adv. Colloid Interface Sci. , 209.
2. AbdElhady M.(2012): Preparation and characterization of chitosan/zinc oxide nanoparticles for imparting antimicrobial and UV protection to cotton fabric. International journal of carbohydrate chemistry, 2012.
3. Adams C.J., Haddow M.F., Hughes R.J., Kurawa M.A. & Orpen A.G.(2010): Coordination chemistry of platinum and palladium in the solid-state: Synthesis of imidazole and pyrazole complexes. Dalton Transactions, 39(15), 3714-3724.
4. Ahmed H., Zuky M. & Badawi A.(2017): Investigation of Novel Tetrahalometallate Complexes
5. of Cetrimonium Bromide Surfactant against in vitro Human Tumour Cell Lines of Lung, Colon and Liver. Annual Research & Review in Biology. , 21(4), 1-9.
6. Akhila J.S., Shyamjith D. & Alwar M.(2007): Acute toxicity studies and determination of median lethal dose. Current science, 917-920.
7. Al-Jailawi M.H., Nasir H.M. & Aziz G.M.(2015): Cytotoxic effect of biosurfactants produced by novel thermophillic Geobacillus thermoleovorans (JQ 912239). Int J Adv Res, 3, 632-637.
8. Baruah H., Barry C.G. & Bierbach U.(2004): Platinum-intercalator conjugates: from DNA-targeted cisplatin derivatives to adenine binding complexes as potential modulators of gene regulation. Current topics in medicinal chemistry, 4(15), 1537-1549.
9. Betanzos-Lara S., Salassa L., Habtemariam A., Novakova O., Pizarro A.M., Clarkson G.J., Liskova B., Brabec V. & Sadler P.J.(2012): Photoactivatable organometallic pyridyl ruthenium (II) arene complexes. Organometallics, 31(9), 3466-3479.

10. Bhadra P., Mitra M., Das G., Dey R. & Mukherjee S.(2011): Interaction of chitosan capped ZnO nanorods with Escherichia coli. Materials Science and Engineering: C, 31(5), 929-937.
11. Brennan N.F. (2005). Structural studies of thallium (I) thourea complexes. University of Pretoria.
12. Chatterjee K., Sarkar S., Jagajjanani Rao K. & Paria S.(2014): Core/shell nanoparticles in biomedical applications. Advances in colloid and interface science, 209, 8-39.
13. Chung R.-J., Wang H.-Y. & Wu K.-T.(2014): Preparation and characterization of Fe-Au alloy nanoparticles for hyperthermia application. J. Med. Biol. Eng, 34(3), 251.
14. Dandekar P., Dhumal R., Jain R., Tiwari D., Vanage G. & Patravale V.(2010): Toxicological evaluation of pH-sensitive nanoparticles of curcumin: acute, sub-acute and genotoxicity studies. Food and chemical toxicology, 48(8-9), 2073-2089.
15. Ezzoukhry Z., Louandre C., Trécherel E., Godin C., Chauffert B., Dupont S., Diouf M., Barbare J.C., Mazière J.C. & Galmiche A.(2012): EGFR activation is a potential determinant of primary resistance of hepatocellular carcinoma cells to sorafenib. International journal of cancer, 131(12), 2961-2969.
16. Ferlay J., Soerjomataram I., Dikshit R., Eser S., Mathers C., Rebelo M., Parkin D.M., Forman D. & Bray F.(2015): Cancer incidence and mortality worldwide: sources, methods and major patterns in GLOBOCAN 2012. International journal of cancer, 136(5), E359-386.
17. Ghosh M.(1984): Toxicity studies. Fundamentals of experimental pharmacology.
18. Hodge A. & Sterner B. (2005). Toxicity Classes In: Canadian Centre for Occupational Health and safety. Copyright@ 1997-2010.

19. Ismail H.M.(1991): A thermoanalytic study of metal acetylacetonates. Journal of analytical and applied pyrolysis, 21(3), 315-326.
20. Jayasuriya A.C., Aryaei A. & Jayatissa A.H.(2013): ZnO nanoparticles induced effects on nanomechanical behavior and cell viability of chitosan films. Materials science & engineering. C, Materials for biological applications, 33(7), 3688-3696.
21. Kärber G.(1931): Beitrag zur kollektiven Behandlung pharmakologischer Reihenversuche. Naunyn-Schmiedebergs Archiv für experimentelle pathologie und pharmakologie, 162(4), 480-483.
22. Kayser O., Lemke A. & Hernandez-Trejo N.(2005): The impact of nanobiotechnology on the development of new drug delivery systems. Current pharmaceutical biotechnology, 6(1), 3-5.
23. Koglin E., Tarazona A., Kreisig S. & Schwuger M.(1997): In-situ investigations of coadsorbed cationic surfactants on charged surfaces: a SERS microprobe study. Colloids and Surfaces A: Physicochemical and Engineering Aspects, 123, 523-542.
24. Kuhn P.-S., Pichler V., Roller A., Hejl M., Jakupec M., Kandioller W. & Keppler B.(2015): Improved reaction conditions for the synthesis of new NKP-1339 derivatives and preliminary investigations on their anticancer potential. Dalton Transactions, 44(2), 659-668.
25. Kura A.U., Saifullah B., Cheah P.-S., Hussein M.Z., Azmi N. & Fakurazi S.(2015): Acute oral toxicity and biodistribution study of zinc-aluminium-levodopa nanocomposite. Nanoscale research letters, 10(1), 105.
26. Law W.-C., Yong K.-T., Roy I., Xu G., Ding H., Bergey E.J., Zeng H. & Prasad P.N.(2008a): Optically and magnetically doped organically modified silica nanoparticles as efficient magnetically guided biomarkers for two-photon

imaging of live cancer cells. The Journal of Physical Chemistry C, 112(21), 7972-7977.

27. Law W.-C., Yong K.-T., Roy I., Xu G., Ding H., J. Bergey E., Zeng H. & Prasad P. (2008b). Optically and Magnetically Doped Organically Modified Silica Nanoparticles as Efficient Magnetically Guided Biomarkers for Two-Photon Imaging of Live Cancer Cells† (Vol. 112).
28. Li Z., Tan S., Li S., Shen Q. & Wang K.(2017): Cancer drug delivery in the nano era: An overview and perspectives. Oncology reports, 38(2), 611-624.
29. Mandal A. & Bishayee A.(2015): Mechanism of breast cancer preventive action of pomegranate: disruption of estrogen receptor and Wnt/β-catenin signaling pathways. Molecules, 20(12), 22315-22328.
30. Murugan E., Jaya Priya R. & Amirthalingam P.(2015): Phase Transfer Catalyst Stabilized Metal Nanoparticles for Free Radical Polymerization. . Int. J. of Research in Chem. and Environ. , 5(1), 96-105.
31. Nair A.S., Vinila V., Issac S., Jacob R., Mony A., Nair H.G., Rajan S., Satheesh D. & Isac J.(2014): Studies on nano crystalline ceramic superconductor LaZrYBaCa2Cu3O11 at three different temperatures. Journal of Crystallization Process and Technology, 4(02), 126.
32. Novakova O., Kasparkova J., Bursova V., Hofr C., Vojtiskova M., Chen H., Sadler P.J. & Brabec V.(2005): Conformation of DNA modified by monofunctional Ru (II) arene complexes: recognition by DNA binding proteins and repair. Relationship to cytotoxicity. Chemistry & biology, 12(1), 121-129.
33. Power E.J., Chin M.L. & Haq M.M.(2018): Breast Cancer Incidence and Risk Reduction in the Hispanic Population. Cureus, 10(2).
34. Quinby M. & Feltham R.D.(1972): Infrared spectra of ruthenium derivatives of nitrogen, nitric oxide, and carbon monoxide. Experimental evidence regarding d. pi.-p. pi. bonding. Inorganic Chemistry, 11(10), 2468-2476.

35. Rahimi R., Mahdavi M., Pejman S., Zare P. & Balalaei S.(2015): Inhibition of cell proliferation and induction of apoptosis in K562 human leukemia cells by the derivative (3-NpC) from dihydro-pyranochromenes family. Acta Biochimica Polonica, 62(1).
36. Randhawa M.A.(2009): Calculation of LD50 values from the method of Miller and Tainter, 1944. J Ayub Med Coll Abbottabad, 21(3), 184-185.
37. Rilda Y., Kurniawan S. & Arief S.(2015): Synthesis and Modification of the Morphology of Zinc Oxide (ZnO) Nano Particles with Induced Biopolymer Chitosan. RESEARCH JOURNAL OF PHARMACEUTICAL BIOLOGICAL AND CHEMICAL SCIENCES, 6(4), 1511-1518.
38. Sadollahkhani A., Kazeminezhad I., Lu J., Nur O., Hultman L. & Willander M.(2014): Synthesis, structural characterization and photocatalytic application of ZnO@ ZnS core–shell nanoparticles. RSC Advances, 4(70), 36940-36950.
39. Sanguinetti A., Polistena A., Lucchini R., Monacelli M., Galasse S., Avenia S., Triola R., Bugiantella W., Cirocchi R. & Rondelli F.(2016): Male breast cancer, clinical presentation, diagnosis and treatment: Twenty years of experience in our Breast Unit. International journal of surgery case reports, 20, 8-11.
40. Sounderya N. & Zhang Y.(2008): Use of core/shell structured nanoparticles for biomedical applications. Recent Patents on Biomedical Engineering, 1(1), 34-42.
41. Todd R.C. & Lippard S.J.(2009): Inhibition of transcription by platinum antitumor compounds. Metallomics, 1(4), 280-291.
42. Vierrether O., TerBush J. & Wisner C.(2016): Nano-Particle TEM Sample Preparation Primer. Microscopy and Microanalysis, 22(S3), 1914-1915.
43. Warrell D.(1995): Clinical toxicology of snakebite in Africa and the Middle East/Arabian Peninsula. Handbook of clinical toxicology of animal venoms and poisons, 433-492.

44. Xiong G., Pal U., Serrano J., Ucer K. & Williams R.(2006): Photoluminesence and FTIR study of ZnO nanoparticles: the impurity and defect perspective. physica status solidi c, 3(10), 3577-3581.
45. Ypsilantis K., Karkabounas S., Georgiou E., Zelovitis I. & Garoufis A.(2014): Synthesis, characterization and interactions with the oligonucleotide d (5′-CGCGAATTCGCG-3′) 2, of bis (terpyridine) ruthenium (II)–peptide conjugates. Inorganica Chimica Acta, 421, 152-159.
46. Zhou L., Qi X., Jiang X., Zhou Y., Fu H. & Chen H.(2013): Organophilic worm-like ruthenium nanoparticles catalysts by the modification of CTAB on montmorillonite supports. Journal of colloid and interface science, 392, 201-205.